PCCP

Accepted Manuscript

ROYAL SOCIETY OF CHEMISTRY

www.rsc.org/pccp

Impact of Constitution of the Terthiophene-Vinylene Conjugated Side Chain on the Optical and Photovoltaic Properties of Two-Dimensional Polythiophenes

Chuen-Yo Hsiow,[a] Rathinam Raja,[b] Chun-Yao Wang,[a] Yu-Hsiang Lin,[c] Yu-Wen Yang,[a] Yen-Ju Hsieh,[a] Syang-Peng Rwei,[c] Wen-Yen Chiu,*[a,d] Ching-I Huang,*[a] Leeyih Wang*[a,b]

[a]Institute of Polymer Science and Engineering, National Taiwan University, 10617 Taipei, Taiwan

[b]Center for Condensed Matter Sciences, National Taiwan University, 10617 Taipei, Taiwan

[c]Institute of Organic and Polymeric Materials, National Taipei University of Technology, 10608 Taipei, Taiwan

[d]Department of Chemical Engineering, National Taiwan University, 10617 Taipei, Taiwan

Email: ycchiu@ntu.edu.tw; chingih@ntu.edu.tw; leewang@ntu.edu.tw

■ Abstract

The effects of the spatial arrangement of the conjugated side chains of two-dimensional polymers on their optical, electrochemical, molecular-packing, and photovoltaic characteristics were investigated. Accordingly, novel polythiophenes with horizontally (**PBTTTV-h**) and vertically (**PBTTTV-v**) grafted terthiophene-vinylene (TTV) conjugated side chains were synthesized that display two and one UV-vis peaks, respectively; the difference is due to the different constitutions of the conjugated side-chains. Because the spatial arrangement affects the molecular self-assembly, **PBTTTV-h** shows stronger crystallinity than **PBTTTV-v**, which enhances the charge mobility in devices. Moreover, **PBTTTV-h** has a lower HOMO energy level (−5.49 eV) than **PBTTTV-v** (−5.40 eV). Bulk heterojunction solar cells fabricated from **PBTTTV-h**/$PC_{71}BM$ and **PBTTTV-v**/$PC_{71}BM$ exhibit power conversion efficiencies of 4.75% and 4.00%, respectively, and V_{oc} values of 800 and 730 mV, respectively, under AM1.5G illumination (100 mW cm^{-2}). Thus, the architecture of the TTV conjugated side chains affects

the optical, electrochemical, and photovoltaic properties; this study provides more ideas for improving 2D conjugated polymers for semiconductor devices.

■ INTRODUCTION

Over the past few decades, conjugated polymers have been rapidly and intensively developed for applications in various types of organic electronics such as field effect transistors (FETs), photo-detectors, light-emitting diodes (LEDs), and polymer solar cells (PSCs).[1-7] PSCs, one of the most interesting organic electronics, have attracted enormous research interest from both academia and industry in recent years because they have the advantages of light weight, low material cost, good mechanical flexibility, and simplicity of manufacture; these characteristics lead to the potential realization of next-generation renewable energy sources.[8-12]

Among the π-conjugated polymers designed as electron-donor materials in bulk heterojunction (BHJ) solar cells, polythiophene derivatives (PTs) have become the most common derivatives in PSCs because of their high charge mobility, strong absorption in the visible region, and synthetic accessibility.[10, 13-19] One of the most studied polythiophenes, i.e., regioregular poly(3-hexylthiophene) (rr-P3HT), has high hole mobility because of its highly oriented semicrystalline structure; however, its relatively high HOMO energy level limits the open-circuit voltage (V_{oc}) of PSC devices.[2, 17] Therefore, the design and synthesis of highly crystalline PTs with broad absorption bands and low-lying HOMO energy levels are crucial for the fabrication of high-performance PSCs.

Many structural designs for novel, diverse, and functional conjugated PTs with low-lying

HOMO energy levels, such as pull–push pairs and incorporation of conjugated side chains, have been reported.[14] Conjugated polymers with conjugated side chains on the polymer backbone have been synthesized and are known as two-dimensional (2-D) conjugated polymers.[14] The vinylene linkage between the polymer backbone and conjugated side chain in 2-D conjugated polymers enhances the coplanarity of the polymer backbone and extends the π-conjugation, resulting in broader absorption, higher hole mobility, and relatively low-lying HOMO energy levels.[20, 21] Li and co-workers reported the incorporation of several kinds of vinylene-linked conjugated side chains into polythiophene backbones, including thienylene-vinylene (TV),[17, 22-25] phenothiazine-vinylene (PV),[26] and styryl-triphenylamine,[27] to extend the π-electron delocalization. Moreover, Tang reported vinylene-linked chromophoric side chains attached to a polythiophene backbone to improve the light-harvesting properties and modify the energy levels of the polymers for PSC devices.[20, 28, 29]

Most previous studies have focused on the design of vinylene-linked 2-D PTs to generate type I TV unit,[20, 23, 29, 30] but less studies discuss about type II TV which is considered against elongation of the π-conjugation (**Figure 1**). However, different constitution of conjugated side chains will change the spatial arrangement and sequence of thiophene rings and thus influence the optical, electrochemical, and crystalline properties of 2-D PTs. Comparing the two regioisomeric structures of thienylene-vinylene, i.e., type I and type II, is interesting and

valuable for the design of conjugated side chains in 2-D PTs.

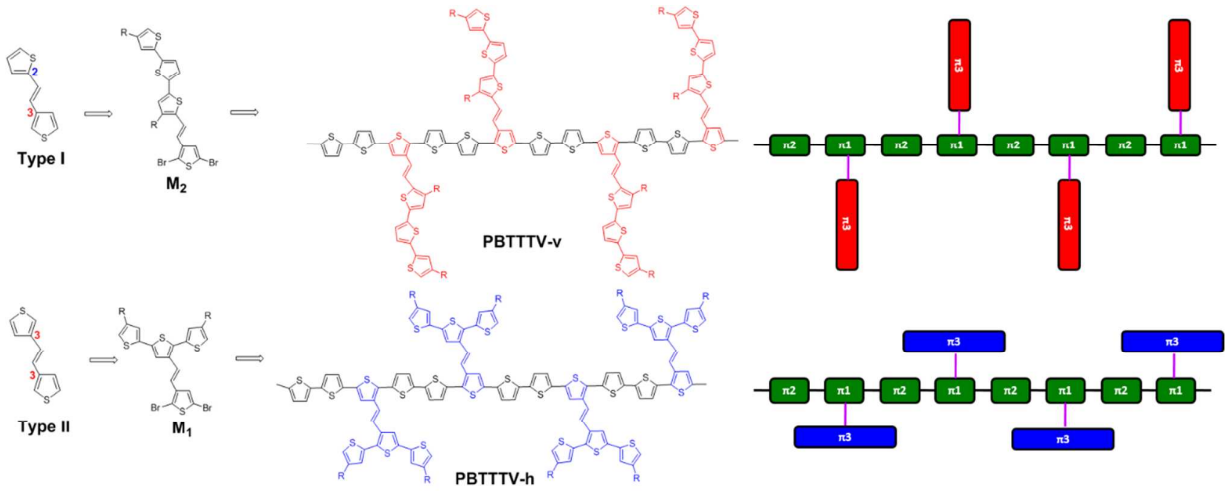

Figure 1. Two types of thienylene-vinylene linkage in 2-D polythiophene.

Herein, we design and synthesize two novel 2-D polythiophenes, i.e., **PBTTTV-h** and **PBTTTV-v**, with horizontally (type II) and vertically (type I) oriented terthiophene-vinylene (TTV) conjugated side chains, respectively, to elucidate the relationship between the isomer polymer structure and the physical properties.

■ EXPERIMENTAL SECTION

Materials. Unless otherwise noted, all nonaqueous reactions were conducted under an atmosphere of nitrogen gas (N_2) in oven-dried apparatus. *P*-xylene and 1,2-dichloroethane were dried over calcium hydride under N_2 prior to use. Tetrahydrofuran (THF) and diethyl ether were distilled over sodium/benzophenone prior to use. *N,N*-dimethylformamide (DMF) was dried over magnesium sulfate ($MgSO_4$) followed by barium oxide (BaO), and stored with molecular sieves in a round-bottom flask under inert atmosphere. Flash chromatography was performed over silica gel (230−400 mesh).

4,4''-Bis(2-ethylhexyl)-2,2':5',2''-terthiophene (1) In a 100 mL two-neck round-bottom flask

with condenser, 2,5-dibromothiophene (1.210 g, 5 mmol), tributyl(4-(2-ethylhexyl)thiophen-2-yl)stannane (5.825 g, 12 mmol) were added. The reaction system was then degassed via vacuum-nitrogen cycle by three times and then 50 ml anhydrous THF was added. $Pd(PPh_3)_4$ (150 mg) in anhydrous THF (10 mL) was added and then refluxed overnight. The reaction mixture was cooled to room temperature and then filtered with Celite to remove the metal catalyst. After removal of the solvent, the residue was purified by column chromatography (eluent: Hexane), yielding a yellow liquid **1** (1.395 g, 2.95 mmol, 59%). ^{1}H NMR (400 MHz, $CDCl_3$) δ 7.03 (s, 2 H), 6.97 (d, 2 H, *J* = 1.6 Hz), 6.77 (d, 2 H, *J* = 1.2 Hz), 2.51 (d, 2 H, *J* = 6.8 Hz), 1.58-1.55 (m, 2 H), 1.36-1.28 (m, 9 H), 0.91-0.89 (m, 7 H); ^{13}C NMR (100 MHz, $CDCl_3$) δ 142.90, 136.58, 136.33, 125.41, 123.87, 119.91, 40.25, 34.57, 32.48, 28.89, 25.61, 23.03, 14.14, 10.83.

4,4''-Bis(2-ethylhexyl)-[2,2':5',2''-terthiophene]-3'-carbaldehyde (2) In a 100 mL two-neck round-bottom flask with condenser, 2,5-dibromothiophene (1.349 g, 5 mmol), tributyl(4-(2-ethylhexyl)thiophen-2-yl)stannane (5.825 g, 12 mmol) were added. The reaction system was then degassed via vacuum-nitrogen cycle by three times and then 50 ml anhydrous THF was added. $Pd(PPh_3)_4$ (150 mg) in anhydrous THF (10 mL) was added and then refluxed overnight. The reaction mixture was cooled to room temperature and then filtered with Celite to remove the metal catalyst. After removal of the solvent, the residue was purified by column chromatography (Hexane: dichloromethane = 1:1), yielding a yellow liquid **2** (1.278 g, 2.88 mmol, 51%). ^{1}H NMR (400 MHz, $CDCl_3$) 10.07 (s, 1 H), 7.50 (s, 1 H), 7.09 (d, *J* = 1.2 Hz, 1 H), 7.02 (s, 1 H), 7.01 (d, *J* = 1.2 Hz, 1 H), 6.82 (s, 1 H), 2.55 (d, *J* = 6.88 Hz, 2 H), 2.51 (d, *J* = 6.88 Hz, 2 H), 1.56-1.54 (m, 2 H), 1.31-1.27 (m, 16 H), 0.90-0.87 (m, 12 H); ^{13}C NMR (100 MHz, $CDCl_3$) 185.03, 146.20, 143.37, 142.99, 137.32, 136.81, 134.97, 131.65, 130.83, 126.54, 124.20, 121.87, 121.19, 40.26, 40.20, 34.42, 34.39, 32.41, 28.81, 25.55, 22.96, 14.07, 10.77.

4,4''-Bis(2-ethylhexyl)-[2,2':5',2''-terthiophene]-5-carbaldehyde (3) In a 100 mL two-neck

round-bottom flask with condenser, the reaction system was then degassed via vacumm-nitrogen cycle by three time. 20 ml anhydrous 1,2-dichloroethane, 0.24 ml anhydrous DMF (3.09 mmol) and 0.28 ml phosphorus oxychloride (3.02 mmol) were added sequentially by syringes at 0 °C. After the reaction mixtures were heated at 90 °C for 1 h, an orange Vilsmeier reagent was formed. Compound **1** (1.5 g, 3.173 mmol) in anhydrous 1,2-dichloroethane (10 mL) was added and then heated at 110 °C for 6 h. The reaction mixture was cooled to 0 °C and then saturated sodium acetate solution and dichloromethane were added slowly. The mixture were extracted twice with 40 ml dichloromethane, then the organic phase was combined, washed several times with saturated sodium acetate solution and water, and dried with $MgSO_4$. After removal of the solvent, the residue was purified by flash column chromatography (eluent: Hexane) , yielding a yellow liquid **3** (1.13 g, 2.19 mmol, 69%). ^{1}H NMR (400 MHz, $CDCl_3$) δ 9.97 (d, 1 H), 7.24 (d, *J* = 4.0 Hz, 1 H), 7.09 (d, *J* = 4.0 Hz, 1 H), 7.02 (d, *J* = 1.6 Hz, 1 H), 7.01 (s, 1 H), 6.84 (d, *J* = 1.2 Hz, 1 H), 2.80 (d, *J* = 7.2 Hz,2 H), 2.50 (d, , *J* = 6.8 Hz, 2 H), 1.67-1.60 (m, 2 H), 1.40-1.28 (m,19 H), 0.95-0.92 (m, 14 H); ^{13}C NMR (100 MHz, $CDCl_3$) 181.60, 153.25, 145.61, 143.17, 139.43, 136.39, 135.91, 134.39, 126.75, 136.69, 126.22, 124.24, 120.91, 41.52, 40.27, 34.53, 32.86, 32.50, 32.46, 28.87, 28.78, 25.72, 25.60, 23.02, 22.96, 14.13, 14.08, 10.83, 10.79.

Diisopropyl ((2,5-dibromothiophen-3-yl)methyl)phosphonate (4)

2,5-dibromo-3-bromomethyl-thiophene[23, 31] (5.0 g, 14.9 mmol) and triisopropyl phosphite (3.4 g, 16.5 mmol) were put in a 50 ml two-neck round-bottom flask with condenser and heated to 160 °C for 5 h. The crude product was purified by flash column chromatography (eluent: hexane:ethylacetate = 3:1) , yielding a colorless liquid **4** (5.80 g, 13.8 mmol, 92%). ^{1}H NMR (400 MHz, $CDCl_3$) 7.05 (d, *J* = 1.2 Hz, 1 H), 4.70-7.60 (m, 2 H), 3.08 (s, 1 H), 3.03 (s, 1 H), 1.30 (d, *J* = 6.2 Hz, 6 H), 1.24 (d, *J* = 6.2 Hz, 6 H). ^{13}C NMR (100 MHz, $CDCl_3$) 132.78, 132.69, 110.78, 110.59, 71.13, 71.06, 29.59, 28.17, 24.07, 24.03, 23.85, 23.81.

(*E*)-3'-(2-(2,5-dibromothiophen-3-yl)vinyl)-4,4''-bis(2-ethylhexyl)-2,2':5',2''-terthiophene (M1) Compound **4** (0.630 g, 1.5 mmol) was taken in a 100 mL Schlenk flask and degassed via vacumm-nitrogen cycle by three times. 20 mL of anhydrous THF was added and stirred in an ice bath for several minutes and then added with sodium *tert*-butoxide (0.115 g, 1.2 mmol). After stirred 30 min, compound **2** (0.500 g, 1 mmol) in anhydrous THF (10 mL) was added. The reaction mixture was warmed to room temperature and stirred overnight. The solution was poured into ammonium chloride aqueous solution and extracted twice with 40 ml hexane. The organic phase was combined and dried with $MgSO_4$. After removal of the solvent, the residue was purified by flash column chromatography (eluent: Hexane) , yielding a pale-yellow liquid **M1** (0.679 g, 0.92 mmol, 92%); ^{1}H NMR (400 MHz, $CDCl_3$) 7.33 (s, 1 H), **7.14 (d, *J* = 16 Hz, 1 H)**, 7.10 (s, 1 H), 7.01 (d, *J* = 0.8 Hz, 1 H), 6.95 (d, *J* = 0.8 Hz, 2 H), **6.85 (d, *J* = 16 Hz, 1 H)**, 6.81 (s, 1 H), 2.57-2.51 (m, 4 H), 1.60-1.25 (m, 18 H), 0.92-0.87 (m, 12 H). ^{13}C NMR (100 MHz, $CDCl_3$) 143.01, 142.86, 139.32, 136.46, 136.00, 135.31, 134.36, 132.89, 127.36, 126.06, 124.46, 122.29, 121.53, 121.21, 120.51, 111.95, 109.91, 40.41, 40.28, 34.60, 34.51, 32.53, 32.49, 29.74, 28.95, 28.90, 25.63, 14.20, 10.92, 10.87.

(*E*)-5-(2-(2,5-dibromothiophen-3-yl)vinyl)-4,4''-bis(2-ethylhexyl)-2,2':5',2''-terthiophene (M2) Using the same procedure as described above for **M1**, the monomer **M2** was synthesized with the yield of 73%, yellow liquid (0.538 g, 0.73 mmol); ^{1}H NMR (400 MHz, $CDCl_3$) 7.13 (s, 1 H), 7.08 (d, *J* = 4.0 Hz, 1 H), 7.05 (d, *J* = 3.6 Hz, 1 H), **7.01 (d, *J* = 16.0 Hz, 1 H)**, 6.98 (d, *J* = 1.2 Hz, 1 H), 6.90 (s, 1 H), 6.80 (d, *J* = 0.8 Hz, 1 H), **6.70 (d, *J* = 16.6 Hz, 1 H)**, 2.60-2.48 (m, 4 H), 1.37-1.29 (m, 18 H), 0.92-0.87 (m, 12 H). ^{13}C NMR (125 MHz, $CDCl_3$) 142.98, 142.42, 139.10, 136.92, 136.44, 135.77, 135.19, 134.95, 127.11, 126.61, 125.58, 124.41, 124.04, 122.50, 120.17, 118.68, 111.92, 109.44,, 41.01, 40.27, 34.56, 32.79, 32.56, 32.48, 28.98, 28.89, 25.79, 25.61, 23.05, 23.03, 14.17, 14.14, 10.96, 10.84.

PBTTTV-h. 5,5'-bis(trimethylstannyl)-2,2'-bithiophene (196.7mg, 0.40 mmol) was weighted

into a 50 ml two neck round-bottom flask and subjected to three successive cycles of vacuum followed by refilling with nitrogen. Then monomer **M1** (295.5 mg, 0.40 mmol) and Pd_2dba_3 (0.01 mmol)/P(*o*-tol)$_3$ (0.02 mmol) were separately dissolved in anhydrous *p*-xylene and added into the reaction mixture via a syringe. The polymerization was carried out at reflux temperature for 48 hr. The raw product was precipitated into methanol and collected through a Soxhlet thimble by filtration, which was then subjected to Soxhlet extraction with methanol, acetone, hexanes, cyclohexane and chloroform. The final polymer was recovered from chloroform fraction by rotary evaporation as purple solid and dried in vacuum for 12 h at 60 °C, yielding **PBTTTV-h** (215 mg, 72%). ^{1}H NMR (400 MHz, $CDCl_3$) δ 7.2-6.4 (br, 8 H), 2.7-2.1 (br, 4 H), 1.5-0.6 (br, 30 H).

PBTTTV-v is synthesized according to the same procedure as mentioned above for PBTTTV-**h.** Reaction of **M2** (236.4 mg, 0.32 mmol) and 5,5'-bis(trimethylstannyl)-2,2'-bithiophene (157.4 mg, 0.32 mmol), yielding **PBTTTV-v** (157 mg, 66%). ^{1}H NMR (400 MHz, $CDCl_3$) δ 7.2-6.4 (br, 8 H), 2.7-2.1 (br, 4 H), 1.6-0.6 (br, 30 H).

Characterization.

^{1}H NMR and ^{13}C NMR spectra were recorded at 400 MHz on Bruker DRX-400 spectrometer. All NMR spectra were calibrated by chloroform-*d* ($CDCl_3$) where ^{1}H NMR chemical shifts of tetramethylsilane is 0 ppm or $CDCl_3$ is 7.26 ppm; in addition, ^{13}C NMR of $CDCl_3$ is 77.0 ppm. The peak multiplicity was described as follows: s = singlet, d = doublet, t = triplet, q = quartet, p = pentet, dd = doublet of doublets, m = multiplet and br = broad. Low resolution electron ionization mass spectra (EI mass) were collected using a Finnigan TSQ 700 and Low resolution electrospray ionization mass spectra (ESI mass) were collected using THERMO Q Exactive Plus FINNIGAN and LCQ Mass Spectrometer. Ultraviolet-visible absorption (UV-vis) spectra were recorded on a JASCO MD-2010 spectrometer. Gel permeation chromatography (GPC) was conducted at 40 ˚C using two Jordi DVB mixed-bed

columns (250×10 mm; suitable for separating polymers with molecular weights from 1×10^2 to 1×10^7 $gmol^{-1}$) using THF as the eluent at a flow rate of 1.0 ml/min on a JASCO instrument that was equipped with UV-vis and refractive index (RI) detectors connected in series. The X-ray diffraction patterns were measured by BRUKER D8 ADVANCED diffactometter operated at a 40 kV voltage and 40 mA current with Cu Kα radiation (λ = 1.542 Å, scan rate: 0.8 s/step). The electrochemical cyclic voltammetry was recorded on CH Instruments CHI 614A With Pt, Pt plate, Ag/Ag^+ as working, counter and reference electrode, respectively, in 0.10 M $(n\text{-}Bu)_4NPF_6$ acetonitrile at scan rate 100 mV/s. For calibration, the redox potential of ferrocene/ferrocenium (Fc/Fc^+) was measured under the same conditions. Theoretical molecular simulation of the studied polymers were calculated through quantum mechanical package Gaussian 03. The molecular geometric structures of the dimers were optimized using the density functional theory method with the B3LYP functional and the 6-31G* basis set.

Device Fabrication.

The polymer solar cells (PSCs) were fabricated in a configuration of the traditional sandwich structure with an indium tin oxide (ITO) glass as anode and a metal as cathode. The ITO glasses were cleaned by a sequential ultrasonic treatment in detergent, deionized water, acetone, and isopropanol for 20 min. Then PEDOT:PSS was filtered through a 0.2-μm filter and spin-coated at 3500 rpm for 30 s on top of ITO electrode. Subsequently, the PEDOT:PSS film was baked at 140 °C for 10 min in the air, and then moved into a glovebox. The blend solution of $PC_{71}BM$ and synthesized polymers (**PBTTTV-h** and **PBTTTV-v**) in a chlorobenzene solvent was filtered through a 0.45-μm filter and spin-coated at 800 rpm for 30 s on top of the PEDOT:PSS layer. These devices were thermally annealed at various temperatures for 10 min, followed by capping with Ca (~20 nm) and then Al (~60 nm) in a thermal evaporator at a base pressure of ca. 10^{-6} Pa. The active area of the devices is 0.06 cm^2. The current density − voltage (J − V) measurements of the devices were conducted on a

computer-controlled Keithley 2400 Source Measure Unit under AM1.5G simulated solar irradiation at 100 mWcm^{-2}. The light incident intensity was calibrated by a mono-Si reference cell with a KG5 filter (PV Measurements, Inc.), which was pre-calibrated by the National Renewable Energy Laboratory. The SCLC measurements were carried out using a Keithley 2400 source meter under dark condition. The IPCE spectra were recorded under illumination by a xenon lamp and a monochromator (TRIAX 180, JOBIN YVON), and the light intensity was calibrated by using an OPHIR 2A-SH thermopile detector.

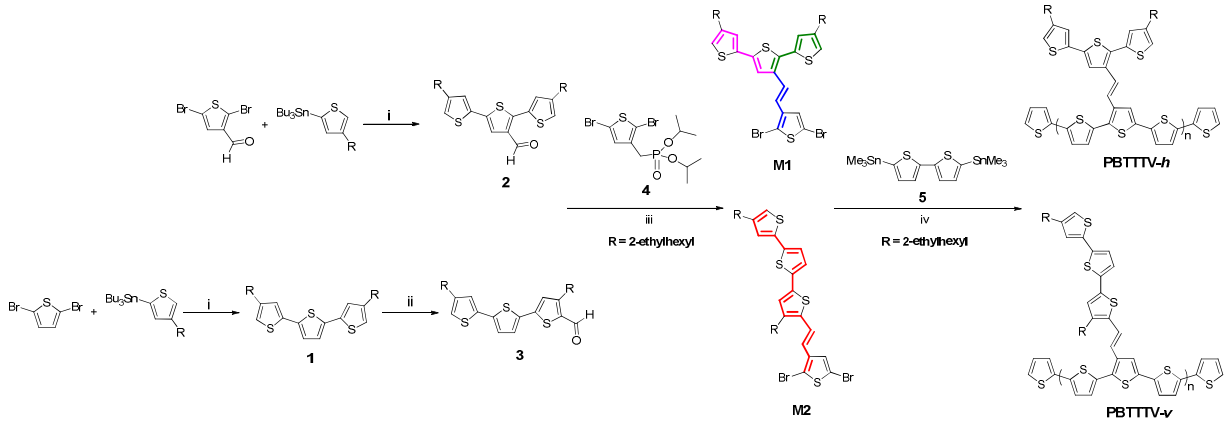

Scheme 1. Synthetic Routes for Monomers and Polymers. Reaction conditions: (i) $Pd(PPh_3)_4$, THF, reflux, overnight; (ii) $POCl_3$, DMF, 1,2-dichloroethane, 110 °C (iii) Sodium *tert*-butoxide, THF, rt, overnight; (iv) Pd_2dba_3, P(*o*-tol)$_3$, *p*-xylene, reflux, 48 h; 2-(tri-*n*-butylstannyl)thiophene, 30 min and then 2-bromothiophene, 30 min.

RESULTS AND DISCUSSION

Synthesis of Monomers and Polymers

Scheme 1 depicts the synthetic routes to the two structural isomers of a conjugated brush-like polymer, i.e., **PBTTTV-h** and **PBTTTV-v**, which possess branched and linear (or horizontal and vertical) conjugated TTV side chains, respectively, and their parent monomers, **M1** and **M2**. **M1** and **M2** were synthesized via the Horner-Wadsworth-Emmons reaction of phosphonate and diisopropyl ((2,5-dibromothiophen-3-yl)methyl)phosphonate **4**, which is the reaction product of 2,5-dibromo-3-(bromomethyl)thiophene and triisopropyl phosphite, with 4,4''-bis(2-ethylhexyl)-[2,2':5',2''-terthiophene]-3'-carbaldehyde **2** or 4,4''-bis(2-ethylhexyl)-[2,2':5',2''-terthiophene]-5-carbaldehyde **3**, respectively. Two alkyl moieties, i.e., 2-ethylhexyl, were introduced into both monomers to enhance the solubility of the corresponding final polymers. Molecule **2** was synthesized by Stille-coupling of tributyl(4-(2-ethylhexyl)thiophen-2-yl)stannane and 2,5-dibromothiophene-3-carbaldehyde in the presence of a catalytic amount of $Pd(PPh_3)_4$. A two-step process was employed to generate **3**: the Stille reaction of tributyl(4-(2-ethylhexyl)thiophen-2-yl)stannane with 2,5-dibromothiophene yielded **1**, which then underwent Vilsmeier formylation with $POCl_3$. The use of a bulky phosphonate as a reagent for the Horner-Wadsworth-Emmons reaction not only enhanced the (*E*)-selectivity but also increased the yield. Coupling constants of ca. 16.0 Hz were observed in the ^{1}H NMR spectra of both **M1** and **M2** (Figures S13 and S14 in the Supporting Information); this clearly demonstrates that the *E*-isomer is the exclusive product for both monomers. Detailed

characterization data for the monomers and intermediates are given in the Supporting Information.

The **PBTTTV-h** and **PBTTTV-v** polymers were prepared via Stille coupling of **M1** and **M2**, respectively, with 5,5'-bis(trimethylstannyl)-2,2'-bithiophene using Pd_2dba_3/P(*o*-tol)$_3$ as the catalyst. Applying 2,2'-bithiophene as the comonomer reduced the steric hindrance of the bulky side chains on **M1** and **M2**. The raw products were precipitated into methanol and collected through a Soxhlet thimble by filtration and then subjected to consecutive Soxhlet extractions with methanol, acetone, hexane, and cyclohexane to remove the small molecules and oligomers and finally with chloroform to obtain the target compounds. Both polymers have comparable yields of ca. 70% and exhibit good solubility in common solvents such as tetrahydrofuran (THF), chloroform, chlorobenzene (CB), and *o*-dichlorobenzene (*o*DCB). Moreover, gel-permeation chromatography (GPC) analyses showed that the two polymers have very similar molecular weight characteristics with number-average molecular weights of around 27 kDa with respect to polystyrene standards (**Table 1**). The high solubility and high molecular weight are essentially due to the two branched 2-ethylhexyl chains on terthiophene.

Optical Properties

The optical properties of the monomers and polymers were examined by UV-vis absorption spectroscopy. As shown in **Figure 2(a)**, although **M1** and **M2** are structural isomers, the latter exhibited a significantly red-shifted absorption spectrum with a maximum at 420 nm; this indicates

that the linear arrangement of the thiophene rings, as compared with the corresponding branched structure, effectively extended the conjugation length of the molecule. For the polymers, the dilute solution of **PBTTTV-h** synthesized from the branched monomer, **M1**, possessed two distinct absorption bands with comparable heights that encompassed wavelengths from 300 to 650 nm. The high-energy (short wavelength) band that peaked at ~340 nm originated from the terthiophene side chain while the low-energy band that peaked at ~530 nm corresponds to the π–π* transition of the conjugated backbone. In contrast, the **M2**-derived polymer, **PBTTTV-v**, exhibited a broad absorption band that peaked at ~443 nm with a weak shoulder peak at ~540 nm, corresponding to the conjugated side chain and polymer main chain, respectively. It should be noted that the absorption coefficient at 530 nm of **PBTTTV-h** is 35.2 $Lg^{-1}cm^{-1}$ (see Figure S26 in the Supporting Information), which is close to that of **PBTTTV-v** (32.5 $Lg^{-1}cm^{-1}$).

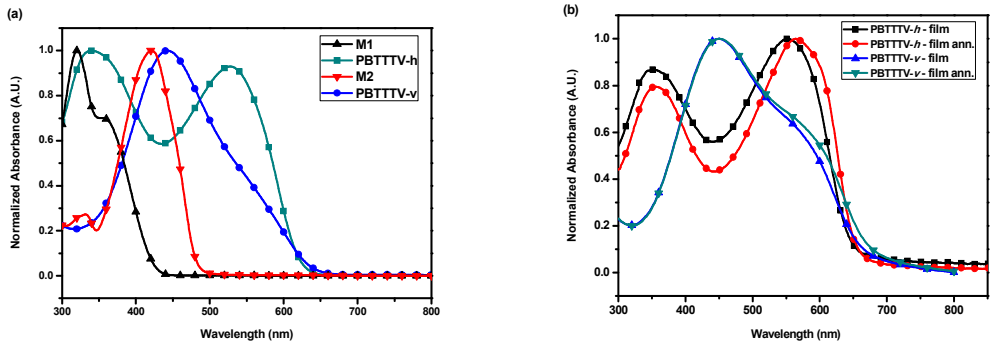

Figure 2. UV−Vis absorption spectra of (a) monomers and polymers in dilute CB solution at room temperature; (b) polymers as spin-coated thin film before and after thermal annealing at 120 ℃ for 15 min.

Figure 2(b) shows that the spin-coated films of both polymers preserved similar absorption characteristics as their parent solutions. The low-energy band of the **PBTTTV-h** film was shifted by about 22 nm to the long-wavelength region corresponding to interchain association in the solid state and improved co-planarity of the backbone.[32] After thermal treatment at 120 °C for 15 min, it underwent a further red-shift of ~13 nm along with the formation of a small shoulder peak, which implies the self-organization of polymer main chains. On the other hand, a relatively small red-shift of ca. 7 nm was observed for the absorption maximum of the **PBTTTV-v** film; moreover, the thermal annealing process had little effect on shifting the peak position of the absorption band. These facts indicate the spatial orientation of conjugated side groups is a decisive parameter affecting the packing behavior of polythiophenes and the vertically anchored TTV branches significantly lower the co- planarity of thiophenes rings in the main chain and hinder the thermally driven self-organization of polymer backbones into ordered structure. Additionally, the optical band-gaps determined from the onset absorption of the spectra of the **PBTTTV-h** and **PBTTTV-v** annealed films were 1.91 and 1.84 eV, respectively.

Table 1. Molecular weight and optical properties of **PBTTTV-h** and **PBTTTV-v**

Polymer	M_w[a] (kDa)	M_n[a] (kDa)	PDI	λ_{max} (nm)			λ_{onset} (nm)	E_g^{opt} (eV)
				Solution[b]	Film[c]	Film, annealed[d]	Film, annealed	Film, annealed[e]
PBTTTV-h	106.4	27.0	3.94	341, 530	345, 552	355, 565	651	1.91
PBTTTV-v	109.2	27.6	3.96	443	450	450	675	1.84

[a]M_w, M_n, and PDI of the polymers were estimated by GPC using polystyrene as standards in THF. [b]Measured in dilute CB solution (10^{-3} g/L). [c]Measured on quartz glass substrate by polymers spin-coated from CB solution (10 g/L). [d]Thermal annealing at 120 °C for 15 min. [e]Estimated from the onset wavelength of the absorption spectra: $E_g^{opt} = 1240/\lambda_{onset}$.

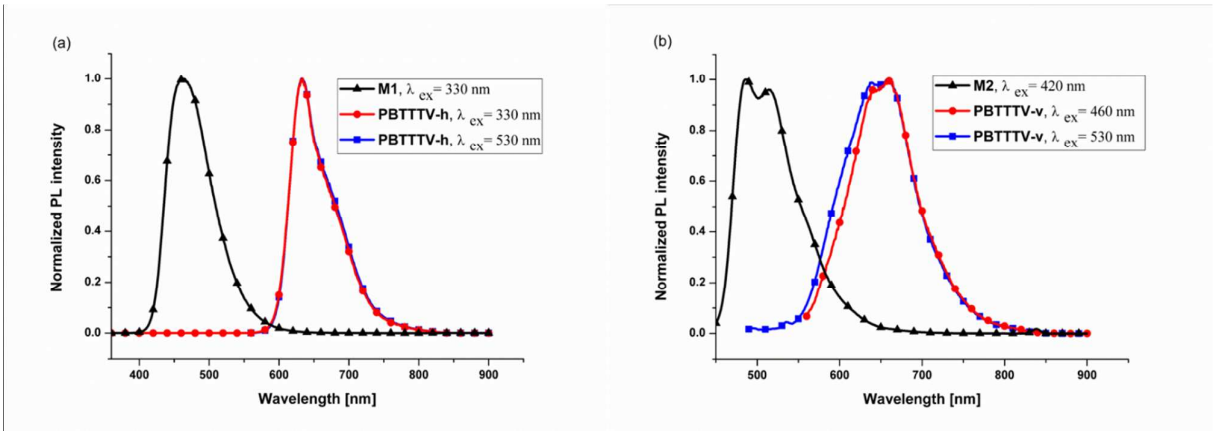

Figure 3. Photoluminescence spectra of (a) **M1** and **PBTTTV-h**; (b) **M2** and **PBTTTV-v** in dilute CB solution at room temperature.

The photoluminescence (PL) spectra of **M1**, **M2**, **PBTTTV-h**, and **PBTTTV-v** in dilute CB solution were recorded at room temperature under excitation at their maximum absorption wavelengths. **Figure 3(a)** shows that the dilute **M1** solution under excitation at 330 nm exhibited a single emission band with a maximum intensity at ~463 nm; the **PBTTTV-h** solution exhibited a red-shifted PL spectrum with a maximum intensity at ca. 634 nm as it is excited at 530 nm which is the absorption maximum wavelength corresponding to the conjugated backbone. Interestingly, as the **PBTTTV-h** solution is excited with a 330 nm incident light, its emission spectrum is different from that of M1 but completely overlaps with that of **PBTTTV-h** taken under 530 nm excitation. Similar behavior was also observed for the **PBTTTV-v** system. The PL of **M2** under excitation at 420 nm showed two emission peaks at ca. 488 and 516 nm. On the other hand, both 460-nm and 530-nm excited PL spectra of the **PBTTTV-v** solution were red-shifted from that of its parent monomer, **M2**, with emission maximum peaks at ca. 657 and 661 nm, and overlap with each other

over most wavelengths with a slight difference in the high-energy region. Such findings clearly indicate highly efficient intramolecular excitation energy transfer from the TTV conjugated side chains to the polymer backbone in these brush-like conjugated polymers.[26, 33, 34] Although **PBTTTV-v** and **PBTTTV-h** have the same chemical structure in terms of main chain, our UV-vis results demonstrate that the spatial arrangement of conjugated TTV branches considerably disturbs the conjugation length and chain conformation of polymer backbone. Moreover, the optimized geometries of both polymers from DFT calculations indicate their theoretical electron-density distributions and energy levels are also affected by the geometry of side chains, as shown in Figure 7. Therefore, a significant difference in the emission characteristics of the two polymers is understandable.

Thin-Film Crystallinity and Charge-Carrier Mobility

The molecular organizations of these polymers in thin solid-state films were investigated using X-ray diffraction (XRD) technique. As shown in **Figure 4**, a broad, weak diffraction peak was detected for the **PBTTTV-v** film before and after thermal annealing, which reveals that it was an amorphous-like compound and the thermal motion of the molecules was insufficient to generate ordered polymer chains packing. Interestingly, the self-assembly behavior of such polymers can be tuned by varying the spatial arrangement of the terthiophene side chains on the polythiophene backbone. In contrast to most side chain-containing conjugated polymers, the as-cast film of **PBTTTV-h** exhibited a visible diffraction peak at $2\theta = 3.79°$ (fitting figures are shown in **Figure**

S27 and **Figure S28**); thermal annealing of the film at 120 °C for 15 min substantially increased the intensity of this peak and shifted the diffraction angle to 2θ = 3.53°. These observations demonstrate that vertically grafted bulky terthiophenes may sterically hinder intra- and intermolecular alignment into a well-organized structure; however, terthiophene units that were horizontally oriented with respect to the backbone facilitated crystallization of the polymer chains into a lamellar structure.

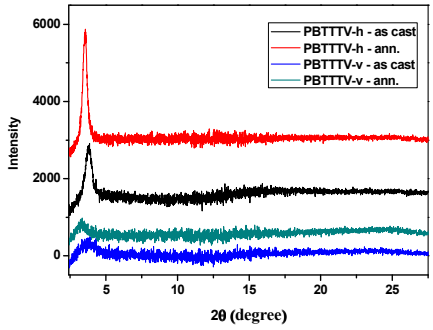

Figure 4. X-ray diffraction patterns of the polymer films by as cast with/without annealing at 120 °C for 15 min.

To gain insight into the crystalline structure, both the *d*-spacing parameter and grain size were determined from the diffraction peaks using Bragg's and Scherrer's equations,[35] respectively. The results are summarized in **Table 2**. The **PBTTTV-h** lamellae in the as-cast film had a grain size of 16.2 nm with a *d*-spacing of 2.33 nm, which is larger than the reported lamellar *d*-spacing of P3HT (~1.64 nm)[36, 37] because of the presence of bulky conjugated side chains between the polymer main chains in **PBTTTV-h**. Although the vertical size is larger in **v**-oriented **TTV** than in **h**-oriented

TTV, the tilt angle of the side chain relative to the polymer backbone is also a decisive factor in determining the *d*-spacing of the lamellae. Tilting the side chain from the upright direction will result in the reduction of the lamellar distance. The XRD results in Table 2 reveal that **PBTTTV-v** and **PBTTTV-h** exhibit comparable *d*-space values. This is probably because the steric hindrance caused by the two alkylthienyl terminal groups in **h**-oriented **TTV** severely limits its maximum reachable tilting angle. Therefore, the **PBTTTV-v** has a wider angle distribution that lowers the average lamellar distance and the grain size of crystallite. Moreover, the annealing process effectively promotes the growth of crystals that results in a significant increment in grain size to 22.1 nm. The slight elongation in *d*-spacing is probably due to the thermal stretching of alkyl moieties on the TTV side chains.[38, 39]

Table 2. Observed *d*-Spacing, FWHM, and grain size from XRD for **PBTTTV-h** and **PBTTTV-v**.

	As-cast films				Thermally annealed films			
	2θ (degree)	*d*-spacing (nm)	FWHM (degree)	Grain size (nm)	2θ (degree)	*d*-spacing (nm)	FWHM (degree)	Grain size (nm)
PBTTTV-h	**3.79**	**2.33**	**0.49**	**16.2**	**3.53**	**2.50**	**0.36**	**22.1**
PBTTTV-v	**3.84**	**2.30**	**2.09**	**3.8**	**3.39**	**2.61**	**1.44**	**5.5**

The hole mobilities of **PBTTTV-h** and **PBTTTV-v** were measured in a hole-only device (ITO/PEDOT:PSS/polymer sample/Au) using the space-charge–limited current (SCLC) method. For comparison, a control experiment on P3HT was also conducted. Figure S24 (Supporting Information) shows a plot of the dependence of the measured current density on the applied voltage; the mobilities, which are listed in Table S5, were calculated according to the following formula[40]:

$$J = \frac{9}{8}\epsilon_r\epsilon_0\mu_0\frac{V^2}{L^3}exp\left(0.89\sqrt{\frac{V}{E_0 L}}\right),$$

where J denotes the current density, ε_r is the dielectric constant of the organic molecule, ε_0 is the permittivity of free space, L is the thickness of the active layer, V is the applied voltage, and E_0 is the characteristic field. The hole mobility of pristine **PBTTTV-h** was determined to be 4.8×10^{-4} $cm^2\ V^{-1}\ s^{-1}$, which is slightly greater than that of P3HT (3.8×10^{-4} $cm^2\ V^{-1}\ s^{-1}$) and about 1.5 times greater than that of **PBTTTV-v** (3.0×10^{-4} $cm^2\ V^{-1}\ s^{-1}$); therefore, it is evident that the formation of an ordered polymer-chain structure improved the carrier mobility of the polymer material.

Electrochemical Properties and Theoretical Calculations

The highest occupied molecular orbital (HOMO) energies were determined using cyclic voltammetry (CV); the results are shown in **Figure 5** and summarized in **Table 3**. CV measurements of as-cast films of the polymers on a Pt electrode were performed at a scan rate of 100 mV s^{-1} in 0.10 M $(n\text{-Bu})_4NPF_6$ acetonitrile solution as the electrolyte using a Pt plate as the counter electrode and $Ag/AgNO_3$ electrode as the reference electrode. The redox potentials were calibrated using a ferrocene/ferrocenium (Fc/Fc^+) redox couple as an external standard.[41] The HOMO energies of the polymers were determined from their onset oxidation potentials ($E_{onset,ox}$) based on the onset oxidation potential of ferrocene (0.46 V, shown in the Supporting Information) as a reference, which is −4.8 V below the vacuum level, according to the following equation[42, 43] : $HOMO = -e(E_{onset,ox} - E_{(Fc/Fc+)} + 4.80)$ (eV). Then, the lowest unoccupied molecular orbital

(LUMO) energies were calculated using the optical band gap (E_g^{opt}) and the calculated HOMO energies according to the following equation: LUMO = HOMO + E_g^{opt} (eV).

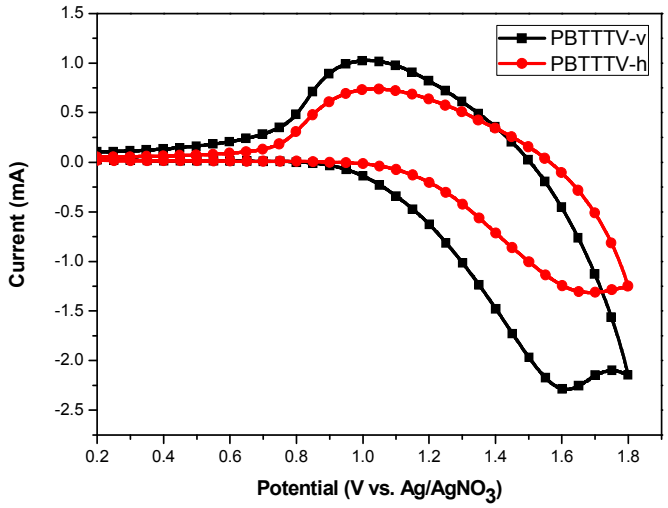

Figure 5. Cyclic voltammograms of as-cast films of **PBTTTV-h** or **PBTTTV-v** on a Pt electrode were carried out at a scan rate of 100 mV s^{-1} in 0.10 M (n-Bu)$_4$NPF$_6$ acetonitrile as the electrolyte: **PBTTTV-h** and **PBTTTV-v**.

The onsets of the oxidation waves for as-cast films of **PBTTTV-h** and **PBTTTV-v** were 1.15 and 1.06 V, respectively, which correspond to HOMO energy levels of −5.49 and −5.40 eV, respectively, and LUMO energy levels of −3.58 and −3.56 eV, respectively. The CV measurements revealed that both **PBTTTV-h** and **PBTTTV-v** had lower HOMO energies than rr-P3HT (ca. −5.0 eV); this would be beneficial for the fabrication of photovoltaic devices with high V_{oc} values.

Table 3. Energy level of **PBTTTV-h** and **PBTTTV-v**

Polymer	$E_{onset,\ ox}$ (V)	$HOMO_{CV}$ (eV)[a]	LUMO (eV)[b]	$HOMO_{cal.}$ (eV)[c]	$LUMO_{cal.}$ (eV)[c]
PBTTTV-h	1.15	−5.49	−3.58	−4.77	−2.09
PBTTTV-v	1.06	−5.40	−3.56	−4.67	−2.22

[a.] Determined from CV data using the equation HOMO = - e($E_{onset,\ ox}$- $E_{(Fc/Fc+)}$ + 4.80) (eV). [b.] LUMO = $HOMO_{cv}$ + E_g^{opt} (eV). [c.] Calculated by the density functional theory (DFT/B3LYP/6-31G/d(p) level).

The CV results demonstrated that the HOMO energy of **PBTTTV-v** was higher than that of **PBTTTV-h**, probably because of the differences in the constitution of the conjugated side chain structures. In other words, comparison of the HOMO energies of **PBTTTV-h** and **PBTTTV-v** revealed that the different spatial arrangements of the terthiophene side chains affected the electron distribution in 2-D PTs. Therefore, we calculated the electron distribution in the molecular structure using density functional theory (DFT) to elucidate the electron delocalization on a molecule; for these calculations, two repeating units (n) were used, and the 2-ethylhexyl group was replaced with a methyl moiety for increased simplicity. **Figure 6** shows the optimized geometry of dimers of **PBTTTV-h** and **PBTTTV-v** calculated at the DFT/B3LYP/6-31G/d(p) level. The dihedral angles of the backbone in the optimized structures of **PBTTTV-h** and **PBTTTV-v** were similar, indicating that the planarities of their backbones were similar. In other words, the different constitutions of the TTV side chains did not significantly affect the planarity of backbone.

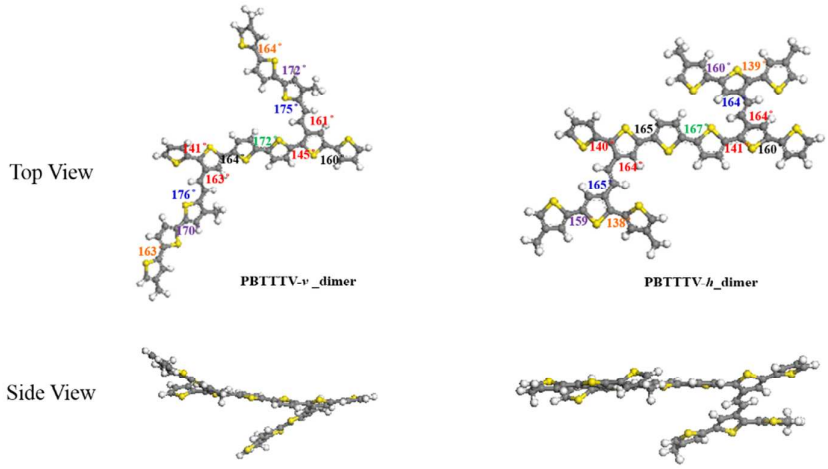

Figure 6. Optimized geometry of top/side view of **PBTTTV-h** and **PBTTTV-v** by the DFT calculation.

Based on the optimized geometries, the results of the electron-density distributions and energy levels of the theoretical calculations are shown in **Figure 7** and the results are summarized in **Table 3**. The trends of variation of the calculated and experimental HOMO energy levels were consistent. More importantly, the conjugated TTV side chain decreased the HOMO energy level while the branched conjugated TTV side chain more effectively reduced the HOMO energy level than the linear one. These results provide a novel route to designing an ideal conjugated polymer with a suitable energy level for organic-semiconductor applications.

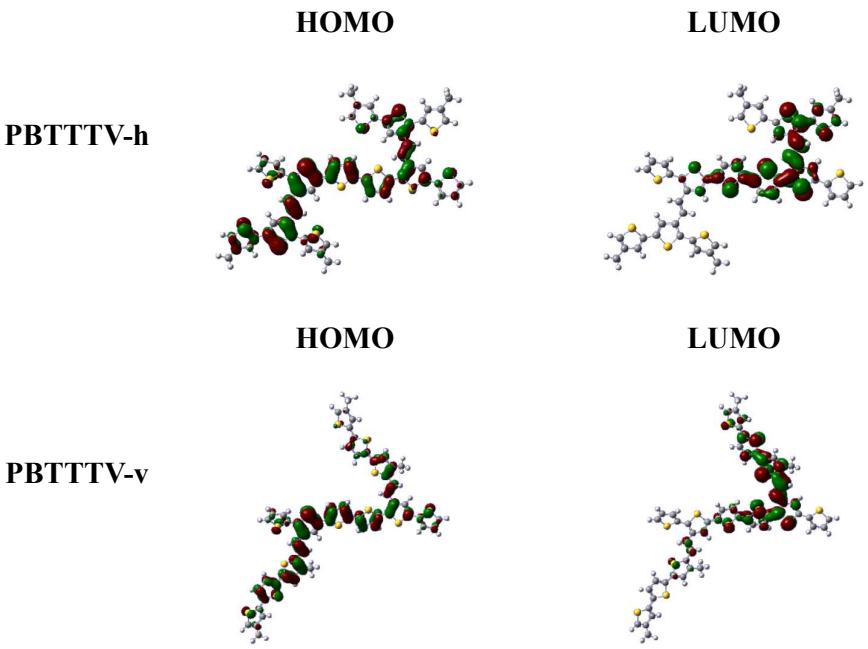

Figure 7. Simulated HOMO, LUMO electron density distributions of **PBTTTV-h** and **PBTTTV-v** by the DFT calculation.

Photovoltaic Properties

Although **PBTTTV-h** and **PBTTTV-v** are structural isomers and have similar molecular weights, they exhibited different light-absorption, self-assembly, and carrier-mobility characteristics. The abilities of the two polymers as electron-donating, hole-transporting, and light-harvesting materials were evaluated by constructing BHJ solar cells with the following configuration: ITO/PEDOT:PSS (40 nm)/polymer:$PC_{71}BM$/Ca (20 nm)/Al (60 nm). The cell performance was optimized by varying the blending ratio of the polymer to $PC_{71}BM$ in the active layer and the temperature at which thermal annealing was executed. The *J–V* curves of these **PBTTTV-h**- and **PBTTTV-v**-based devices are presented in Figures S22 and S23 (Supporting Information),

respectively, and the corresponding photovoltaic data are summarized in Tables S1–S4 (Supporting Information). **Figure 8(a)** shows *J–V* curves of the optimized **PBTTTV-h**/$PC_{71}BM$ and **PBTTTV-v**/$PC_{71}BM$ solar cells. The former device exhibited a short-circuit current density (J_{sc}) of 9.10 mA/cm^2, V_{oc} of 800 mV, and fill factor (*FF*) of 65.2%, leading to a promising PCE of 4.75%; in contrast, the latter device exhibited a comparable J_{sc} of 9.02 mA/cm^2 and slightly lower V_{oc} and *FF* values of 730 mV and 60.8%, respectively, leading to a PCE of 4.00%. For comparison, the PSC device based on P3HT/PC71BM was also fabricated under identical processing conditions. Its *J-V* curve is displayed in **Figure S29** (Supporting Information), exhibiting a J_{sc} of 9.03 mA/cm^2, a V_{oc} of 610 mV, and an *FF* values of 57.4% which is equivalent to a PCE of 3.16%. Obviously, both **PBTTTV-h**/$PC_{71}BM$ and **PBTTTV-v**/$PC_{71}BM$ devices have higher V_{oc} and *FF* values and thereby better PCEs than those of the P3HT/$PC_{71}BM$ device, indicating that the structural design of TTV conjugated side chains is of benefit to the performance enhancement of polymer solar cells.

Further to elucidate the origins of J_{sc}, the dependence of the external quantum efficiencies (EQEs) of both the solar cells on the wavelength of incident light was measured. Both EQE spectra cover a broad wavelength range 300–700 nm and had values greater than 50% between 360 and 600 nm, indicating good efficiency of photon-to-electron conversion. Moreover, the relative EQE values closely followed the relative light-harvesting capabilities of the two polymers; therefore, the **PBTTTV-h**/$PC_{71}BM$ cell had lower EQEs in the region ~300–450 nm and higher EQEs in the region ~450–650 nm than the **PBTTTV-v**/$PC_{71}BM$ cell. In addition, the integrated current densities

determined from the EQE curves of the **PBTTTV-h**/$PC_{71}BM$ and **PBTTTV-v**/$PC_{71}BM$ devices with the AM1.5G solar spectrum were 9.8 and 7.0 mA/cm^2, respectively, which agree well with the J_{sc} values determined from the corresponding *J*–*V* curves.

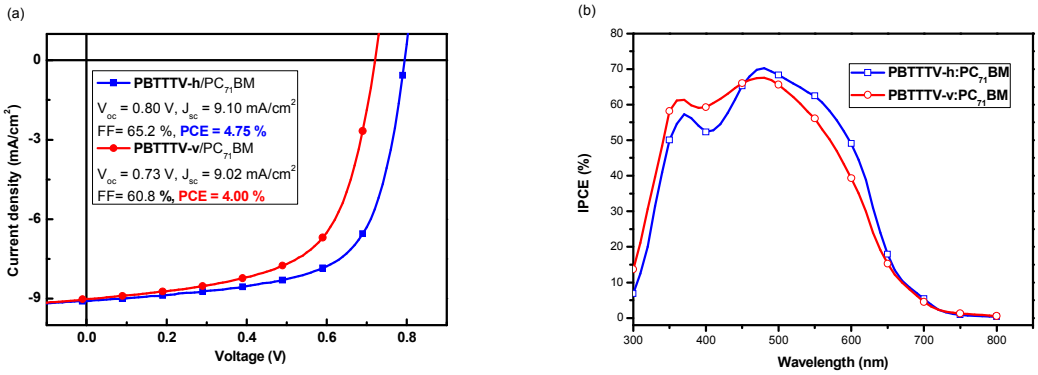

Figure 8. (a) J–V curves (b) IPCE spectra of optimized polymer/fullerene devices

Importantly, because of the low-lying HOMO energy levels of these branched polythiophenes, the V_{oc} values of the **PBTTTV-h**/$PC_{71}BM$ and **PBTTTV-v**/$PC_{71}BM$ solar cells substantially exceeded the commonly reported V_{oc} (~ 0.6 V) for devices based on linear poly(3-hexylthiophene). Basically, the V_{oc} values of the two types of solar cells studied herein correlated with the relative magnitude of the HOMO levels of the corresponding polymer donors; therefore, the **PBTTTV-h**/$PC_{71}BM$ device exhibited a V_{oc} that is ~10% greater than that of the **PBTTTV-h**/$PC_{71}BM$ device. In addition, the former cell noticeably outperformed the latter cell in terms of *FF* because of reduced series resistance and enlarged shunt resistance, suggesting that the greater hole mobility of **PBTTTV-h** not only lowered the resistance to the transport of free holes in the active layer to the anode but also the recombination loss of the charge carriers. These findings

demonstrate that the h-type spatial arrangement of TTV side chains was more effective in enhancing the V_{oc} and *FF* values of BHJ solar cells than the common v-type configuration.

CONCLUSIONS

In summary, two novel polythiophenes with structurally isomeric TTV conjugated side chains, i.e., **PBTTTV-h** (branched) and **PBTTTV-v** (linear), were designed, synthesized, and applied in PSCs. The branched alkyl side chains significantly enhanced the solubility of the polymers, and the unsubstituted bithiophene moieties in the polymer backbone acted as spacers to improve the coplanarity and enhance absorption. Because of the different architectures of the TTV conjugated side chains, **PBTTTV-h**, which contained branched TTV side chains, displayed two distinct absorption peaks in its UV-vis spectrum and was a crystalline polymer, as verified by XRD, which leads to significantly higher charge mobility; in contrast, **PBTTTV-v**, which contained linear TTV side chains, showed a single absorption peak and was an amorphous material. The differences in the molecular spatial arrangement obviously affected the self-assembly and charge mobility of two-dimensional polythiophenes. Moreover, PTs with conjugated side chains decreased the HOMO energy level, and the branched conjugated TTV side chain more effectively reduced the HOMO energy level than the linear one. These results provide a novel route for designing ideal conjugated polymers with suitable energy levels for organic-semiconductor applications. PSCs based on **PBTTTV-h**/$PC_{71}BM$ displayed a PCE of 4.75% and V_{oc} of 800 mV, while those based on **PBTTTV-v**/$PC_{71}BM$ displayed a PCE of 4.00% and lower V_{oc} of 730 mV under AM1.5G illumination (100 mW cm^{-2}). These results not only demonstrate that the different architectures of the TTV conjugated side chains effectively impact the optical, electrochemical, and photovoltaic properties but also provide potential ideas to improve 2-D conjugated polymers for semiconductor devices through structural isomers. Moreover, molecular engineering approach, such as introducing

pull-push pairs and the nature of alkyl side chains, of 2-D conjugated polymers based on **PBTTTV-h** would open a new way for developing high performance organic semiconductor materials.

■ ACKNOWLEDGMENT

The authors thank National Taiwan University, Academia Sinica (AS-103-SS-A02), and the Ministry of Science and Technology of the Republic of China (MOST 102-2113-M-002-003-MY3; MOST 103-3113-E-102-011; MOST 103-2623-E-002-017-ET) for financially supporting this research. The computation resources from the National Center for High-Performance Computing of Taiwan and Computer and Information Networking Center of National Taiwan University.

■ NOTE and REFERENCE

1. J. Mei and Z. Bao, *Chem. Mater.*, 2014, **26**, 604-615.
2. C. Lu, H. C. Wu, Y. C. Chiu, W. Y. Lee and W. C. Chen, *Macromolecules*, 2012, **45**, 3047-3056.
3. P. M. Beaujuge and J. R. Reynolds, *Chemical Reviews*, 2010, **110**, 268-320.
4. A. C. Grimsdale, K. Leok Chan, R. E. Martin, P. G. Jokisz and A. B. Holmes, *Chemical Reviews*, 2009, **109**, 897-1091.
5. J. Mei, Y. Diao, A. L. Appleton, L. Fang and Z. Bao, *Journal of the American Chemical Society*, 2013, **135**, 6724-6746.
6. K. Pu, A. J. Shuhendler, J. V. Jokerst, J. Mei, S. S. Gambhir, Z. Bao and J. Rao, *Nat Nano*, 2014, **9**, 233-239.
7. L. Feng, C. Zhu, H. Yuan, L. Liu, F. Lv and S. Wang, *Chem. Soc. Rev.*, 2013, **42**, 6620-6633.
8. G. Yu, J. Gao, J. C. Hummelen, F. Wudl and A. J. Heeger, *Science*, 1995, **270**, 1789-1791.
9. H.-W. Liu, D.-Y. Chang, W.-Y. Chiu, S.-P. Rwei and L. Wang, *Journal of Materials Chemistry*, 2012, **22**, 15586-15591.
10. Y.-J. Cheng, S.-H. Yang and C.-S. Hsu, *Chemical Reviews*, 2009, **109**, 5868-5923.
11. H. J. Son, B. Carsten, I. H. Jung and L. Yu, *Energy & Environmental Science*, 2012, **5**, 8158-8170.
12. G. Li, R. Zhu and Y. Yang, *Nat Photon*, 2012, **6**, 153-161.

13. A. Facchetti, *Chemistry of Materials*, 2011, **23**, 733-758.
14. Z. Lin, J. Bjorgaard, A. Gul Yavuz, A. Iyer and M. E. Köse, *RSC Advances*, 2012, **2**, 642.
15. J. Roncali, *Accounts of Chemical Research*, 2009, **42**, 1719-1730.
16. H. J. Son, F. He, B. Carsten and L. Yu, *Journal of Materials Chemistry*, 2011, **21**, 18934-18945.
17. Z. G. Zhang, S. Zhang, J. Min, C. Cui, H. Geng, Z. Shuai and Y. Li, *Macromolecules*, 2012, **45**, 2312-2320.
18. B. C. Thompson and J. M. J. Fréchet, *Angewandte Chemie*, 2008, **47**, 58-77.
19. F. Zhang, D. Wu, Y. Xu and X. Feng, *Journal of Materials Chemistry*, 2011, **21**, 17590-17600.
20. Z. Gu, P. Shen, S.-W. Tsang, Y. Tao, B. Zhao, P. Tang, Y. Nie, Y. Fang and S. Tan, *Chemical Communications*, 2011, **47**, 9381-9383.
21. Z. Gu, P. Tang, B. Zhao, H. Luo, X. Guo, H. Chen, G. Yu, X. Liu, P. Shen and S. Tan, *Macromolecules*, 2012, **45**, 2359-2366.
22. Z.-G. Zhang, Y.-L. Liu, Y. Yang, K. Hou, B. Peng, G. Zhao, M. Zhang, X. Guo, E.-T. Kang and Y. Li, *Macromolecules*, 2010, **43**, 9376-9383.
23. J. Hou, Z. a. Tan, Y. Yan, Y. He, C. Yang and Y. Li, *Journal of the American Chemical Society*, 2006, **128**, 4911-4916.
24. J. Hou, C. Yang, C. He and Y. Li, *Chemical Communications*, 2006, 871-873.
25. E. Zhou, Z. a. Tan, Y. Yang, L. Huo, Y. Zou, C. Yang and Y. Li, *Macromolecules*, 2007, **40**, 1831-1837.
26. Y. Zou, W. Wu, G. Sang, Y. Yang, Y. Liu and Y. Li, *Macromolecules*, 2007, **40**, 7231-7237.
27. Z.-G. Zhang, S. Zhang, J. Min, C. Chui, J. Zhang, M. Zhang and Y. Li, *Macromolecules*, 2011, **45**, 113-118.
28. Z. Gu, L. Deng, H. Luo, X. Guo, H. Li, Z. Cao, X. Liu, X. Li, H. Huang, Y. Tan, Y. Pei and S. Tan, *Journal of Polymer Science Part A: Polymer Chemistry*, 2012, **50**, 3848-3858.
29. C. Wang, B. Zhao, Z. Cao, P. Shen, Z. Tan, X. Li and S. Tan, *Chemical Communications*, 2013, **49**, 3857-3859.
30. P. Shen, H. Bin, L. Xiao and Y. Li, *Macromolecules*, 2013, **46**, 9575-9586.
31. Z.-G. Zhang, S. Zhang, J. Min, C. Chui, J. Zhang, M. Zhang and Y. Li, *Macromolecules*, 2012, **45**, 113-118.
32. Z. Zhu, D. Waller, R. Gaudiana, M. Morana, D. Mühlbacher, M. Scharber and C. Brabec, *Macromolecules*, 2007, **40**, 1981-1986.
33. J. Hou, L. Huo, C. He, C. Yang and Y. Li, *Macromolecules*, 2006, **39**, 594-603.
34. L. Dou, J. Gao, E. Richard, J. You, C.-C. Chen, K. C. Cha, Y. He, G. Li and Y. Yang, *Journal of the American Chemical Society*, 2012, **134**, 10071-10079.
35. S. Grecu, M. Roggenbuck, A. Opitz and W. Brütting, *Organic Electronics*, 2006, **7**, 276-286.
36. C.-Y. Chen, C.-S. Tsao, Y.-C. Huang, H.-W. Liu, W.-Y. Chiu, C.-M. Chuang, U. S. Jeng, C.-J. Su, W.-R. Wu, W.-F. Su and L. Wang, *Nanoscale*, 2013, **5**, 7629-7638.
37. T.-A. Chen, X. Wu and R. D. Rieke, *Journal of the American Chemical Society*, 1995, **117**,

233-244.

38. I. Osaka, G. Sauvé, R. Zhang, T. Kowalewski and R. D. McCullough, *Advanced Materials*, 2007, **19**, 4160-4165.
39. D. Qian, W. Ma, Z. Li, X. Guo, S. Zhang, L. Ye, H. Ade, Z. a. Tan and J. Hou, *Journal of the American Chemical Society*, 2013, **135**, 8464-8467.
40. Y.-M. Chang, W.-F. Su and L. Wang, *Solar Energy Materials and Solar Cells*, 2008, **92**, 761-765.
41. Y. Ie, J. Huang, Y. Uetani, M. Karakawa and Y. Aso, *Macromolecules*, 2012, **45**, 4564-4571.
42. M. C. Hwang, J.-W. Jang, T. K. An, C. E. Park, Y.-H. Kim and S.-K. Kwon, *Macromolecules*, 2012, **45**, 4520-4528.
43. K. Asadi, F. Gholamrezaie, E. C. P. Smits, P. W. M. Blom and B. d. Boer, *Journal of Materials Chemistry*, 2007, **17**, 1947-1953.

Graphical Abstract